

The BiomolBiomed publishes an “Advanced Online” manuscript format as a free service to authors in order to expedite the dissemination of scientific findings to the research community as soon as possible after acceptance following peer review and corresponding modification (where appropriate). An “Advanced Online” manuscript is published online prior to copyediting, formatting for publication and author proofreading, but is nonetheless fully citable through its Digital Object Identifier (doi®). Nevertheless, this “Advanced Online” version is **NOT the final version of the manuscript**. When the final version of this paper is published within a definitive issue of the journal with copyediting, full pagination, etc., the new final version will be accessible through the same doi and this “Advanced Online” version of the paper will disappear.

Tomita: Lymphatic and blood vessels in parathyroid tumors

Lymphatic and blood vessels in parathyroid tumors: Immunohistochemical study with LYVE-1 and von Willebrand factor

Tatsuo Tomita

Department of Integrative Biosciences, Oregon Health and Science University, Portland, OR,
USA

Corresponding author: Tatsuo Tomita; tomitat39@gmail.com

DOI: <https://doi.org/10.17305/bb.2024.10547>

Submitted: 01 April 2024/ **Accepted:** 26 July 2024/ **Published online:** 23 August 2024

Conflicts of interest: Author declare no conflicts of interest.

Funding: Author received no specific funding for this work.

ABSTRACT

Parathyroid tumors exhibit distinct histopathological features that differentiate benign from malignant lesions. This study aimed to study characteristic distribution of lymphatic and blood vessels in normal parathyroid gland and parathyroid tumors to distinguish cancer from benign tumors. Immunohistochemical staining for lymphatic and blood vessels and parathyroid hormone was performed with parathyroid proliferating lesions including adenoma, multiglandular multiple adenomas, atypical tumor, and carcinoma. Lymphatic vessels were immunostained with lymphatic vessel endothelial receptor 1(LYVE-1) and blood vessels were immunostained with von Willebrand factor (vWF). Normal parathyroid gland contained several round blood vessels with less linear lymphatic vessels. The less parathormone-immunostained adenomas weighing less than 2 g revealed larger blood vessels with perivascular small linear lymphatic vessels, and the larger adenomas contained proportionally larger blood vessels. Smaller multiglandular multiple adenomas were like smaller adenomas with less parathormone staining and contained larger, round blood vessels with perivascular small linear lymphatic vessels. Larger multiglandular multiple adenomas weighing more than 4g and one atypical tumor contained nodular pattern consisted of alternating strongly parathormone-positive lobes and negative lobes with numerous, dilated blood vessels and perivascular linear lymphatic vessels. Both primary and metastatic carcinomas were strongly and diffusely positive for parathyroid hormone with numerous lymphatic and blood vessels at the invading margin. Thus, normal parathyroid has rich blood vessels which provide accessibility of minced tissues seeding for auto-transplantation. Immunostaining patterns of parathyroid hormone, lymphatic and blood vessels help to distinguish carcinoma from benign parathyroid proliferating lesions. The negative immunohistochemical staining for parafibromin will detect carriers of hyperparathyroidism-jaw tumor (HPT-JT) syndrome and would help in diagnosing parathyroid cancer in both HPT-JT carriers and sporadic patients.

Keywords: Adenoma, Blood Vessels, Carcinoma, Immunohistochemistry, Lymphatic Vessels, Lymphatic vessel endothelial receptor 1(LYVE-1), Parathyroid

INTRODUCTION

This study aims to investigate the characteristic distribution of lymphatic and blood vessels in normal parathyroid glands and hyperfunctioning parathyroid lesions, including adenoma, multiglandular multiple adenoma (MMA), atypical tumors, and primary and metastatic carcinoma. The goal is to distinguish between benign and malignant tumors (1, 2). Currently, commercially available markers for lymphatic vessels include PROX-1 (prospero-related homeobox-1), LYVE-1 (lymphatic vessel endothelial hyaluronic acid receptor-1), podoplanin (a 43 kDa membrane glycoprotein of podocytes), and VEGFR-3 (vascular endothelial growth factor receptor-3). LYVE-1 is a transmembrane receptor for hyaluronan, which is highly expressed by lymphatic vessels (3-8). Podoplanin is a membrane glycoprotein found on the surface of rat glomerular epithelial cells (podocytes), recognized by the monoclonal antibody D2-40 (3). These markers bind to their specific sites in different modes and function diversely at various stages of tissue growth and development (3). The markers for blood vessels include CD31 (platelet endothelial cell adhesion molecule, PECAM-1, found on endothelial cells), CD34 (a transmembrane sialomucin protein used for hematopoietic progenitor cells, positive in blood vessel endothelium but not in lymphatic vessel endothelium), and von Willebrand factor (vWF, which binds to factor VIII, a coagulation factor, aiding in platelet aggregation and adhesion to the vessel wall). These are all pan-endothelial markers (4). However, there are no specific markers exclusively for lymphatic and blood vessels (3-9). LYVE-1 was chosen as a marker for lymphatic vessels and vWF for blood vessels.

The parathyroid glands are well-vascularized, primarily receiving their arterial blood supply from the inferior thyroid artery. Venous blood from these glands drains into the internal jugular and brachiocephalic veins. (10, 11). As endocrine glands with rich vasculature, parathyroids have the ability to spontaneously induce angiogenesis in vitro (12-14) and in vivo (4).

Hyperproliferating parathyroid lesions, including adenoma, MMA, and atypical tumors, are generally less immunostained for parathyroid hormone (PTH) and chromogranin A (CgA) compared to normal parathyroid tissue. This corresponds to less stored PTH and CgA in tumor tissues due to autonomous hypersecretion (2, 15). The 2022 WHO classification of parathyroid tumors reclassified multiglandular parathyroid hyperplasia as MMA, as affected parathyroids are usually composed of multiple clonal neoplastic proliferations (1). In auto-transplanted normal parathyroids post-thyroidectomy, the transplanted tissues grow in the forearm subcutis and

muscle pocket (16-18). Despite the known rich lymphatic and vasculature in PG, the histopathological evidence of lymphatic and blood vessels has not been thoroughly investigated. By immunohistochemical staining for lymphatic vessels with LYVE-1 and for blood vessels with CD34, Garcia et al. reported an increase in lymphatic vessels in parathyroid adenomas and MMA compared to normal glands (19). Endocrine glands are generally richly vascularized to secrete hormones in tandem, maintaining critical hormone pulses and homeostasis via complex feedback mechanisms, regulated by blood concentrations of various hormones (20), glucose, electrolytes, and other serum components. For instance, pancreatic islets, which constitute only 1—2% of the pancreatic tissue mass, play a crucial role in regulating blood glucose levels by secreting insulin. Despite their small size, they receive a significant 10—15% of the pancreas's total blood supply. (21). Immunostaining pancreatic tissue with vWF reveals pancreatic islets as numerous, round baskets of entangled capillaries, distinct from the surrounding exocrine pancreatic tissue (22). Parathyroid tissues, being relatively small, are well-preserved in formalin-fixed and paraffin-embedded tissues and are suitable for immunohistochemical staining of lymphatic and blood vessels. Immunohistochemical staining with frozen sections yields better results for lymphatic and blood vessels than with formalin-fixed and paraffin-embedded tissue sections using these markers (22).

MATERIALS AND METHODS

Normal human parathyroids from five euparathyroid patients were collected at autopsy. Parathyroids from patients with primary hyperparathyroidism were surgically resected at the University of Kansas Medical Center, Kansas City, Kansas, during my tenure there. The primary hyperparathyroidism tissues included twelve adenomas, six MMAs, one atypical tumor, and two carcinomas. The 2022 WHO classification reclassified atypical adenoma as an atypical tumor and multiglandular hyperplasia as MMA (1). The tissues were routinely fixed in 10% neutral formalin and embedded in paraffin. To inhibit endogenous peroxidase activity, sections were incubated with a solution containing glucose oxidase (1 U/ml) and sodium azide (10 mmol/ml) for 45 minutes at 25°C (22). Sections were then incubated with blocking serum for 20 minutes. Next, sections were incubated with a 1:100 diluted primary antibody solution of goat anti-human LYVE-1 (R & D System, Minneapolis, MN), rabbit anti-human vWF (Dako System, Carpinteria, CA), and monoclonal anti-human PTH antibody (Dako System), overnight at 4°C.

After rinsing and immersion in blocking serum again, sections were incubated with the second antibody (1:200 dilution) for 30 minutes at room temperature. The final visualization was achieved using the ABC kit (Vector Laboratories, Burlingame, CA) and 0.025% diaminobenzidine tetrahydrochloride (Dojindo Molecular Technologies, Rockville, MD) in a Tris-buffer at pH 7.6, with 0.03% H₂O₂ added to produce a brown color (15,22). The immunostained tissue slides of larger proliferative lesions were examined at 10x magnification, with the field measuring 1.96 mm² for estimating the sizes of lymphatic and blood vessels. The sizes of lymphatic and blood vessels were classified as follows: extra-large vessels (larger than 1,000 μm x 500 μm), large vessels (500 μm x 200 μm), medium-sized vessels (200 μm x 50 μm), small vessels (120 μm x 15 μm), and the smallest vessels (50 μm x 15 μm).

RESULTS

One case each of normal parathyroid, adenoma, and MMA is presented in Figure 1. In five normal PGs, each gland weighed 30 to 60 mg, with the total weight of the four glands being 150 ± 22 mg and the tissue section sizes measuring 0.5 ± 0.3 cm (Table 1). The normal parathyroid glands were diffusely and strongly positive for PTH (Fig. 1-B). In Case 5, the normal PG with about 20% fibroadipose tissue (Fig. 1-A), measured 0.8 x 0.5 cm and weighed 30 mg, and was diffusely and strongly immunostained for PTH (Fig. 1-A and -B). The parathyroid contained the smallest lymphatic vessels (50 μm x 15 μm) and several round blood vessels (200 μm x 50 μm) with many small linear blood vessels (Fig. 1-C and -D). In Case 2 adenoma, which measured 1.4 cm x 0.6 cm and weighed 1g, a normal rim measuring 0.3 cm x 0.2 cm and containing 50% fibroadipose tissue was attached. There were a few small, linear lymphatic vessels (50 μm x 15 μm) and a dozen small, linear blood vessels (120 μm x 15 μm) between the rim and the adenoma (Fig. 1-E and -F). In Case 2 MMA, one of four glands, measuring 1.2 cm x 0.7 cm and weighing 2g in a total of 4.5 g in four glands (Table 1), there were numerous small linear lymphatic vessels and dilated round blood vessels (500 μm x 200 μm) (Fig. 1-G and -H). Generally, the sizes of blood vessels were proportionally larger for larger adenomas. Among the twelve adenomas, a total of four glands varied in weight from 0.5 g to 4.8 g, with a mean of 2.1 ± 0.4 g (Table 1). Case 7 adenoma, measuring 2.0 x 1.5 cm and weighing 4.8 g, was

contiguous to a rim of normal gland tissue. It was composed of amphophilic cytoplasm and a prominent nucleus and was less immunostained for PTH (Fig. 2-A and -B). Large, dilated blood vessels (1,000 μm x 500 μm) with perivascular small linear lymphatic vessels were found between the normal gland and the adenoma (Fig. 2-C and -D). The adenoma contained many small linear lymphatic and blood vessels (Fig. 2-C and -D). MMAs varied in weight from 1.5 g to 7.5 g in four glands, with a mean of 4.3 ± 1.2 g (Table 1).

Cases 5 and 6, weighing 7.5 g in four glands, consisted of nodular patterns with occasional calcification in the fibrous stroma (Fig. 2-E). There were alternating strongly PTH-immunostained lobules and PTH-negative lobules (Fig. 2-F). Large, dilated veins (1,000 μm x 500 μm) were found at the tumor margin with perivascular linear lymphatic vessels (Fig. 2-G and -H). Glands weighing less than 7.5 g showed less PTH-immunostaining, with moderately increased blood vessels attached to linear lymphatic vessels, as seen in Case 7 adenoma (Fig. 2-B). The sizes of blood vessels were larger in proportion to the sizes of the tumors.

The atypical tumor, measuring 1.5 x 1.2 cm and weighing 4.5 g (Table 1), was composed of two different immunostaining lobules: the mostly peripherally located small cell lobules consisting of small, dark, round to oval nuclei and scanty cytoplasm, and the major mid-portion lobules consisting of larger ampholytic cells with slightly larger nuclei and twice the amphophilic cytoplasm as the small cell lobules, separated by thin to thick fibrous bands (Fig. 3-A). The peripherally located small cell lobule was diffusely and strongly immunostained for PTH, while the major mid-lobules were negatively stained for PTH, with a few scattered PTH-immunostained cells (Fig. 3-B). There were aggregates of small lymphatic vessels in the deep thick fibrous band (Fig. 3-C), while several round, enormously large, dilated blood vessels (> 1,000 μm x 500 μm) and many small blood vessels were present in the thin fibrous stroma between the peripheral lobules and major mid-portion lobules of the tumor (Fig. 3-C and -D). Thus, there was no lymphatic and blood vessel proliferation at the peripheral margin of the atypical adenoma. Similar large blood vessels with perivascular linear lymphatic vessels were also present in larger adenomas (Cases 6 and 10), weighing ≥ 3.6 g (Table 1).

Case 1 primary carcinoma, measuring 1.8 x 1.5 cm and weighing 6 g (Table 1), consisted of large eosinophilic cytoplasm and large nuclei with prominent nucleoli. The tumor invaded the

neck skeletal muscle and connective tissue, forming nodular tumor lobules separated by thin fibrous bands (Fig. 4-A) and was diffusely and strongly positive for PTH (Fig. 4-B). Several of the smallest, linear lymphatic vessels (50 μm x 15 μm) and several small blood vessels were found at the infiltrating tumor margin (Fig. 4-C and -D), while no lymphatic or blood vessels were observed in the midst of the tumor (Fig. 4-C and -D). In Case 2 metastatic lymph node, measuring 1.3 x 0.6 cm and weighing 2 g (Table 1), tumor emboli were present at the capsule of the lymph node (Fig. 4-E). Tumor cells consisted of large nuclei and larger eosinophilic cytoplasm with solid, nodular lobules separated by thin fibrous bands, where vascular tumor invasions were present at the tumor margin (Fig. 4-E). The tumor cells were diffusely and moderately positive for PTH (Fig. 4-F). The smallest lymphatic vessels (50 μm x 15 μm) were found in the peripheral fibrous band but not in the mid-portion of the tumor (Fig. 4-G), while several large, dilated, round blood vessels (1,000 μm x 500 μm) were found in the adjacent connective tissue, with numerous small linear venous vessels diffusely distributed in the entire mid-portion of the tumor tissue (Fig. 4-G and -H).

DISCUSSION

In the five normal parathyroids, a few of the smallest lymphatic vessels and several round medium-sized blood vessels were observed. In twelve adenomas, three cases had a normal rim attached (Table 1). The normal parathyroid contained a few lymphatic vessels and several round medium-sized blood vessels (Fig. 1-A and -B), which supports the suitability for auto-transplantation, while lymphatic vessels were very sparse and may not participate in seeding the auto-transplantation of parathyroid glands. Since minced parathyroid tissues may be auto-transplanted in a muscle pocket, there must be ample capillaries in the normal parathyroid (16-18), as also revealed in the numerous capillaries in pancreatic islets (22). Both minced parathyroid tissues and isolated pancreatic islets have been successfully transplanted as vascular-rich tissues (16-18,23-25). In formalin-fixed and paraffin-embedded tissue, small blood vessels, especially capillaries, were not adequately immunostained, and these capillaries were only properly immunostained with frozen sections (22) or using the technique for skin biopsy, where 50 μm thick floating tissue sections make it feasible to immunostain small blood vessels in the fixed tissues (26-28). Each technique is labor-intensive and cumbersome (22, 26-28). After total thyroidectomy for thyroid carcinoma, post-surgical hypoparathyroidism is an inevitable consequence (29, 30). To prevent hypoparathyroidism, auto-transplantation of parathyroid glands

has been widely performed (29-31). Small normal PGs contain several medium-sized blood vessels and numerous capillaries as a vascular endocrine organ, and these normal glands have been successfully auto-transplanted in cases with thyroid carcinoma after thyroidectomy (29, 30). The classical procedure of auto-transplantation of parathyroids is as follows: The resected parathyroids are placed in saline or tissue culture medium at 4°C. After cooling the tissue for 30 minutes, the gland is sufficiently firm to be sliced into 1 mm slices or cubes. Generally, 10 to 20 pieces are inserted into subcutaneous tissue or individual muscle pockets. The incision is closed with non-absorbable suture or clips to assist subsequent identification (29-31). PTH radioimmunoassay will assess the success of parathyroid auto-transplantation by measuring serum PTH levels during and shortly after the surgery (31, 32), as PTH has a short half-life of about 5 minutes (33).

The weight of adenomas varied from 0.5g to 4.8g, with a mean weight of 2.1 ± 0.4 g and a mean size of 1.4 x 0.7 cm (Table 1). Adenomas were less immunostained for PTH than normal glands (Fig. 2-B), and there were increased lymphatic and blood vessels at the tumor margin. In Case 7 adenoma, there was one extra-large blood vessel ($> 1,000 \mu\text{m} \times 500 \mu\text{m}$) and several medium-sized blood vessels between the rim and the adenoma, suggesting active angiogenesis. Increased angiogenesis has been reported in adenomas compared to other proliferative lesions using VEGF and VEGFR-2 as vascular markers (34, 35) and in primary hyperparathyroidism compared to normal glands using CD105 as a vascular marker (35). A dozen small linear lymphatic vessels and several dilated large-sized blood vessels were found between the normal rim and adenoma in Cases 2, 5, and 7 adenomas (Fig. 1-E to -H).

In MMAs, weight varied from 1.5g to 7.5g, with a mean weight of 4.7 ± 1.0 g and a mean size of 1.2 x 0.8cm (Table 1). Large glands contained numerous perivascular small lymphatic vessels and several enormously dilated blood vessels at the margin (Fig. 2-G and -H). These proliferating lymphatic and blood vessels were confined to the parathyroids, indicating the benign nature of proliferation. As seen in Case 2 MMA (Fig. 2-G and -H), there were many extra-large blood vessels, proportionate to the size of the adenoma, and a few dilated and many small perivascular lymphatic vessels at the margin of the adenoma (Fig. 2-C and -D). This supports the concept that blood and lymphatic vessels develop in tandem and independently or together, forming a circulatory system that allows the passage of fluid and the delivery of PTH in

the body (20). Angiogenesis appears to be the main mechanism through which perivascular lymphangiogenesis is coordinated in the angiolympangiogenetic process in normal and benign tumors (12-14). This increased blood vessel presence in adenomas and MMA may support the idea that these tissues, with more blood vessels, are more favorable for auto-transplantation if such a procedure is needed.

The atypical tumor exhibited unique histopathology, consisting of outer PTH-positive small cell lobules and major inner PTH-negative large cell lobules (Fig. 3-B). This outer cluster of small cells, consisting of small dense nuclei and scanty cytoplasm, was also presented in Figure 14 of the atypical parathyroid tumor published by Erickson et al., which had less Ki-67 labeling compared to a higher index in the adjacent tumor cells with larger cytoplasm (36). There were fibrous bands between the outer and inner lobules containing abundant dilated large blood vessels and aggregates of small lymphatic vessels (Fig. 3-C and -D). The absence of lymphatic and blood vessels at the tumor margin supports the benign nature of this tumor, even though it was originally diagnosed as carcinoma with no recurrence 10 years after the initial surgery. This patient presented with high serum calcium (13.5 - 13.9 mg/dl; normal: 8.3 – 10.4 mg/dl), low phosphate (2.1 mg/dl; normal: 3.4 – 4.5 mg/dl), and extremely high serum PTH (569 pg/ml; normal: 10 - 65 pg/ml), with coexisting hypercalcemia and hypophosphatemia, and extremely high levels of serum PTH (37). The laboratory data for this atypical tumor were very similar or identical to that of reported cases of carcinoma, including serum calcium > 12 mg/dl with levels 3-4 mg above the upper normal limit, and significantly elevated PTH levels, usually 10 times the upper limit (38). Thus, laboratory data on increased serum calcium, decreased phosphate, and markedly increased PTH may not differentiate between atypical tumors and carcinoma, requiring histopathological criteria for a definitive diagnosis. Six weeks after tumor resection, serum calcium levels were 8.0 mg/dl and serum PTH was 86.9 pg/ml, with some restoration of normal calcium-PTH balance (38). Angiogenesis observed in adenomas and one atypical tumor was confined to the parathyroid gland and did not extend outside the gland, unlike the evident lymphangiogenesis at the tumor capsule seen in Case 1 primary carcinoma. It is extremely difficult histopathologically to distinguish parathyroid carcinoma from atypical tumors, and active lymphangiogenesis at the invading tumor margin is a definitive sign of malignancy (39, 40).

Case 1 primary carcinoma consisted of diffusely nodular large cell lobules separated by thin fibrous bands, which contained several small lymphatic and blood vessels at the invading tumor margin (Fig. 4-C and -D). This carcinoma invaded the adjacent skeletal muscle and connective tissue, where increased lymphangiogenesis was observed (Fig. 4-A to -D). Large eosinophilic tumor cells with prominent nuclei were diffusely and strongly positive for PTH (Fig. 4-A and -B), suggesting ample PTH-containing secretory granules despite autonomous hypersecretion of PTH (38-40). In Case 2 metastatic lymph node, tumor emboli were present at the lymph node margin (Fig. 4-E), with diffusely distributed small venous vessels throughout the metastatic lymph node, suggesting carcinoma-induced angiogenesis (Fig. 4-H). Large eosinophilic tumor cells with prominent nuclei were diffusely and strongly positive for PTH (Fig. 4-B and -F). Numerous small lymphatic and venous vessels were present at the invading cancer margin, implying cancer-induced lymphangiogenesis in tandem with cancer cell invasion (Fig. 4-G and -H). Akirov et al. recently reported eight cases of parathyroid carcinomas, a relatively large case series from one institution, as the incidence of parathyroid carcinoma is relatively rare. In this series, there were seven cases of vascular invasion (87.5%) and five cases of lung metastasis (62.5%) (37). Thus, vascular invasion and hematogenous metastasis to the lung are very common in parathyroid carcinoma (37). Similar lymphangiogenesis was also observed at the invading mucosal margin of TNM T1 colonic adenocarcinoma (41).

The final diagnosis of malignancy should be based on histopathological criteria of a parathyroidectomy specimen, including: 1) vascular invasion characterized by tumor invading through a vessel wall and associated thrombosis, or intravascular tumor cells admixed with thrombus, 2) lymphatic invasion, 3) perineural invasion, 4) local malignant invasion into adjacent anatomic structures, and 5) histologically/cytologically documented metastasis (1, 36, 37). Proliferating vascular and lymphatic invasion could be added as another sign of cancer diagnosis. Using traditional immunohistochemistry, benign parathyroid adenomas are less immunostained for PTH and CgA compared to normal parathyroids, while normal parathyroids and the majority of parathyroid tumors (81%) are negative for synaptophysin (2,35). A high Ki67 index favors malignancy (1, 37).

Recently, parafibromin deficiency has been expanded upon, and the term "parafibromin-deficient neoplasm" is applied to a neoplasm showing a complete absence of parafibromin

immunostaining in the nucleus (1, 42-45). This "parafibromin deficiency" indicates an underlying biallelic somatic or germline CDC73 (cell division cycle 73) inactivation (1, 42, 46), supporting the diagnosis of carcinoma rather than an atypical tumor (1,42). Syndromic PHP includes multiple endocrine neoplasia 1 to 4 (MEN 1 to 4) and hyperparathyroidism jaw-tumor syndrome (HPT-JT syndrome) (47). HPT-JT syndrome is characterized by parathyroid tumors, fibro-osseous jaw tumors, cystic kidney diseases, and uterine tumors (48). HPT-JT syndrome is autosomal dominant, and carriers of this syndrome develop parathyroid adenoma in late adolescence or early adulthood, with at least 10% to 15% transforming into parathyroid carcinoma from a single adenoma in later years (43, 47). HPT-JT syndrome is due to mutations in CDC73, which encodes parafibromin (47). Up to 10% of patients with HPT-JT below age 45 with nonsyndromic and sporadic HPT may have MEN 1, CDC73, or CASR mutations and will have mutations in one of 11 genes (47). Somatic mutations of CDC73 can be identified in up to 70% of patients with parathyroid carcinoma, with mutations being somatic in one-third of cases (49). The simple absence of immunostaining for parafibromin will detect carriers of HPT-JT syndrome with deficient parafibromin and would aid in diagnosing parathyroid cancer in both HPT-JT carriers and sporadic patients (1). CDC73 functions as a genuine tumor suppressor gene involved in the regulation of p53 and as a component of the human PAF1 complex, which controls RNA polymerase II-mediated transcription (44, 50). Loss of immunohistochemical staining of parafibromin may lead to genetic testing for biallelic CDC73 mutation inactivation in both parathyroid adenoma and carcinoma (1, 43, 47). Since CDC73 mutations are also associated with both HPT-JT syndrome and sporadic parathyroid carcinoma, negative immunostaining for parafibromin may well be used as a marker for all parathyroid carcinomas (1).

Perivascular lymphangiogenesis occurs mostly following angiogenesis, as seen in perivascular small linear lymphatic vessels around the newly formed blood vessels in the current parathyroid proliferative lesions (Figures 2-C, -D, -G, and -H). The formation of lymphatic vessels may rely not solely on lymphangiogenesis but also on angiogenic factors (51, 52). Thus, while tumor-induced lymphangiogenesis often coordinates with angiogenesis, it can also occur independently. For example, malignant lesions in the parathyroid glands can induce lymphangiogenesis without accompanying angiogenesis (52-54). Lymphatic endothelial cells proliferate and migrate, leading to lymphangiogenesis, then proliferating cells and their stroma induce the formation of new lymphatic capillaries by secreting VEGF-C, cytokines, and other molecular families (52-55).

Apparent cancer-induced angiogenesis was observed in two cancerous cases (19,23,34): the primary cancer (Case 1) showed infiltrating lymphangiogenesis into the invading skeletal muscle, and the metastatic lymph node (Case 2) revealed tumor emboli with numerous venous proliferations in the entire lymph node. These rare parathyroid carcinomas present a good example of lymphangiogenesis for spreading cancerous endocrine cells. Tumor-induced angiogenesis responds to the increased blood circulation needed for the proliferating parathyroid lesions.

CONCLUSIONS

Normal parathyroids are equipped with many linear and several round blood vessels, along with smaller and linear lymphatic vessels, supporting the histological suitability of normal glands for auto-transplantation. Proliferative lesions, including single adenomas and MMAs, showed adenoma-induced lymphangiogenesis, where lymphatic vessels were confined within the capsule and fibrous bands or around proliferating blood vessels within the parathyroids. Laboratory data, including serum calcium, phosphate, and PTH, may not differentiate between atypical tumors and carcinomas, and histopathological criteria are still required for differentiation.

Many lymphatic and small blood vessels were proliferating at the invading tumor margin in primary carcinoma, while hematogenous spread in the metastatic lymph node revealed diffuse small venous vessel proliferation throughout the lymph node. Thus, lymphangiogenesis is a limited pattern in benign tumors, while primary carcinoma induces profound lymphangiogenesis at the infiltrating cancer margin in tandem with spreading cancerous tissues. The hematogenous metastatic lymph node was accompanied by diffuse vascular proliferation. Therefore, proliferating lymphangiogenesis is a diagnostic and prognostic marker for parathyroid malignancy. Negative immunostaining for parafibromin will detect carriers of HPT-JT syndrome and help diagnose parathyroid cancer in both HPT-JT carriers and sporadic patients.

REFERENCE

1. Erickson, LA, Mete, O, Juhlin, CC, Perren, A, Gill, AJ: Overview of the 2022 classification of parathyroid tumors. *Endocr Pathol* 2022, 33(1):64-89.
2. DeLellis, RA: Parathyroid tumors and related disorders. *Mod Pathol* 2011, 24(3): s78-s93.

3. Kong, LL, Yang, NZ, Shi, LH, Zhao, GH, Zhou, W et al: The optimum marker for the detection of lymphatic vessels (Review). *Mol Cell Oncology* 2017, 7 (4):515-520.
- 4 Muller, AM, Hermanns, MI, Skrzynski, C, Nesslinger, M, Muller, KM et al: Expression of the endothelial markers PECAM-1, vWF and CD34 in vivo and in vitro. *Exp Mol Pathol* 72(3);221-229.
5. Scavelli, C, Weber, E, Agliano, M, Cirulli, T, Nico, B et al: Lymphatics at the crossroads of angiogenesis and lymphangiogenesis. *J Anat* 2004, 204 (6):433-449.
6. Pusztaszeri, MP, Seelentag, W, Bosman, FT: Immunohistochemical expression of endothelial markers CD31, CD34, von Willebrand factor, and Fli in normal human tissues. *J Histochem Cytochem* 2006, 54(94):385-395.
7. Jackson, DG, Prevo, R, Clasper, S, Bonerji, S: LYVE-1, the lymphatic system and tumor lymphangiogenesis. *Trend Immunol* 2001, 22 (6):317-321.
8. Jackson, DG: The lymphatics revisited. New perspectives from the hyaluronan receptor LYVE-1. *Trend Cardiovasc Med* 2003, 13 (1): 1-7.
9. Tammela, T, Alitalo, K: Lymphangiogenesis: Molecular mechanisms and future promise. *Cell* 2010, 140 (4): 460-476.
10. Norobi, M, Saiki, S, Tanaka, N, Harihara, Y, Shindo, S et al: Blood supply of the superior parathyroid artery. *Surgery* 1999, 115(4):417-423.
11. Gill, Z, Patel, SG: Surgery for thyroid cancer. *Surg Oncol Clin N Am* 2008, 17(1):93-120.
12. Saxe, A: Parathyroid transplantation: A review. *Surgery* 1984,95(5):507-526.
13. Lazarus, AC, Tseleni-Balafouta, S, Papatomas, T, Brousalis, T et al: Immunochemical investigation on angiogenic factor in parathyroid proliferating lesions. *Eur J Endocrinol* 2006, 154(6): 827-833.
14. Segiet, OA, Pichaliski, M, Brzodowa-Zozowa, M, Piecuch, A, Zaba, M et al: Angiogenesis in primary hyperthyroidism. *Ann Diag Pathol* 2015, 19(2):91-98.
15. Tomita, T: Significance of chromogranin A and synaptophysin in parathyroid proliferative lesions: Immunohistochemical study on parathyroid adenoma, atypical adenoma, carcinoma, and hyperplasia. *Open Access J Endocrinol*. 2022, 6(1):1-13.
16. Barczynski, M, Golkowski, F, Newrot, I Parathyroid transplantation in thyroid surgery. *Gland Surg* 2017, 6(5):530-536.

17. Agarwal, A, Waghray, A, Gupta, S, Sharma, P, Milas, M. Cryopreservation of parathyroid tissue: An illustrated technique using the Cleveland Clinic protocol *J Am Coll Surg* 2013, 216(1): e1-e9.
18. Borot, S, Lapierre, V, Carnalille, B, Coudet, P, Ponfornis, A: Results of cryopreserved parathyroid autographs: A retrospective multicenter study. *Surgery* 2010 147(4):529-535.
19. Garcia, N, Torre de la, I, Buley, I, Wass, JAH, Jackson, DG, Turner, HE Angiogenesis and lymphangiogenesis in parathyroid proliferative lesions. *J Clin Endocrinol Metab* 2004 89 (6):2890-2896.
20. Schaeffer, M, Hodson, DJ, Lafont, C, Mollard, P. Endocrine cells, and blood vessels work tandem to generate hormone pulses. *J Mol Endocrinol* 2011, 47(2): R59-R
21. Jansson, L, Barbu, A, Bodin, B, Drott, CJ, Espes, D et al Pancreatic blood flow and its measurement. *Ups J Med* 2016, 12 (2):81-95.
22. Tomita, T: Immunohistochemical staining for lymphatic and blood vessels in normal organs. Comparison between paraffin-embedded tissues and frozen sections. *Acta Med Acad* 2021, 50(1):13-28.
23. Warnock, GL, Meloche, RM, Thompson, D, Shapiro, RJ, Fung, M et al: Improved human pancreatic islet isolation prospective cohort study of islet transplantation vs best medical therapy in type 1 diabetes mellitus. *Arch Surg* 2005, 140(8):735-744.
24. Ludwig, B, Reichel, A, Steffen, A: Transplantation of human islets without immunosuppression. *Proc Natl Acad Sci* 2013, 110(47):19054-19058.
25. Rickels, M, Robertson, RD: Pancreatic islet transplantation in humans: Recent progress and future directions. *Endocr Rev* 2019, 40(2):631-668.
26. McArthur, JC, Stocks, EA, Hauer, P, Cornblath, DR, Griffin, JW: Epidermal nerve fiber density. *Arch Neurol* 1998, 55(12):1513-1520
27. Ebenezer, GS, Hauer, P, Gibbons, C, McArthur, JC, Polydefkis, M: Assessment of epidermal fibers: A new diagnostic and predictive for peripheral neuropathies. *J Neuropath Exp Neurol* 2007, 66(12):1059-1073.
28. Saperstein, DS, Levine, TD, Hank, N: Usefulness of skin biopsy in the evaluation and management of patients with suspected small fiber neuropathy. *Int J Neurosci* 2013, 123(1):38-41.
29. Hicks, G, George, R, Sywak, M: Short and long-term impact of parathyroid auto transplantation on parathyroid function after total thyroidectomy. *Gland Surg* 2017 (Suppl 1): s75-s85.

30. Wang, B, Zhu, CR, Liu, H, Wu, J: The effectiveness of parathyroid gland auto transplantation in preserving parathyroid function during thyroid surgery for thyroid neoplasms. *PLOS One*, 2019, 14(8): e221173.
31. Bieglmayer, C, Prager, G, Niederle, B: Kinetic analysis of parathyroid hormone clearance as measured by three immunoassay during parathyroidectomy. *Clin Chem* 2002, 48(10):1731-1738.
32. Richards, ML, Bingener-Casey, J, Pierce, D, Strodel, WE, Sirinek, KR: Intraoperative parathormone assay: An accurate predictor of symptomatic hypocalcemia following thyroidectomy. *Arch Surg* 2003, 138(6):632-636. 33.
- Marchens, A, Lorenz, K, Drable, H: Parathyroid hormone levels predict long-term outcome after operative management of parathyroid cancer. *Horm Metab Res* 2017, 49(7):485-492. 34.
35. Chorti, A, Cheva, a, Chatzkyriakidou, A, Achilla, C, Boulogeorgou, K et al: Sporadic parathyroid adenoma: an updated review of molecular genetics. *Front Endocrinol (Lausanne):*, 2023, May8:14:118211.
35. Louzaris, AL, Tseleni-Balafuta, S, Papathomas, T, Bousalis, T, Thompoulos, G et al: Immunohistochemical investigation of angiogenic factor in parathyroid proliferative lesions. *Eur J Endocrinol* 2006, 154(6):827-833.
36. Erickson, LA, Mete, O: Immunohistochemistry on diagnostic pathology. 2018, *Endocr Pathol* 2018, 29(2):113-129.
37. Akirov, A, Asa, SL, Larouche, V, Mete, O, Sawka, M, et al: Clinicopathological spectrum of parathyroid carcinoma. *Front Endocrinol* 2019, 00731.
38. Tomita, T: Immunocytochemical staining patterns for parathyroid hormone and chromogranin in parathyroid hyperplasia adenoma, and carcinoma. *Endocr Pathol* 1999, 10(2):145-156.
39. Carlson, D: Parathyroid pathology. *Hyperparathyroidism and parathyroid tumors. Arch Pathol Lab Med* 2010, 134(11):1639-1644.
40. Duan, K, Gomez Hernandez, K, Meta, O: Clinicopathological correlates of hyperparathyroidism. *J Clin Pathol* 2025, 68(10):771-787.
41. Tomita, T: Cancer-associated lymphatic and venous vessels in colonic carcinomas. *Open J Pathol* 2014, 4(1):101-109.
42. Juhlin, CC, Nelsson, IL, Lagerstadt-Robinson, K, Stenman, Brandstrom, R, Tham, E et al: Parafibromin immunostaining of parathyroid tumors in clinical routine: a near-decade experience from a tertiary center. *Mod Pathol* 2019, 32(8):1082-1094.

43. Gill, AJ, Lim, G, Cheung, KY, Andrici, L, Perry-Keene, JL et al: Parafibromin-deficient (HPT-JT type, CDC73 mutated) parathyroid tumors demonstrate distinctive morphologic features. *Am J Surg Pathol* 2019, 43(1):35-46.
44. Storvall, S, Leijon, H, Ryhanen, EM, Vesterinen, T, Heiskanen, I et al: Flamin A and paraformin expression in parathyroid carcinoma. *Eur J Endocrinol* 2021, 185(6):803-812.
45. Gao, Y, Wang, P, Lu, J, Pan, B, Guo, D et al: Diagnostic significance of paraformin expression in parathyroid carcinoma. *Human Pathol* 2022, 127(1):28-38.
46. Jo, JH, Chung, TM, Youn, H, Yo, JY: Cytoplasmic parafibromin /hCDC73targets and destabilizes p53 mRNA to control p53-mediated apoptosis. *Nat Commun* 2014, 12:5433.
47. Skefos, CM, Waguespack, SG, Perrier, N, Hu, MI, Adam, MP et al: CDC73 related disorders. *Genetic Rev Univ Washington, Seattle, 2023, Sep. 21.*
48. Thakker, RV.: Genetics of parathyroid tumours. *J Int Med* 2016, 280(6):574-583.
49. Salcuni, AS, Calani, F, Guarnierri, V, Nicastro, V, Romagnoli, E et al: Parathyroid carcinoma. *Best Prac Res Clin Endocrinol Metab* 2018, 32(6):877-889.
- 50: Xu, Y, Bernecky, C, Lee, CT, Mair, KC, Schwalb, B et al: Aarchitecture of the RNA polymerase II-Paf1V-TFIIs transcription elongation complex. *Nat Commun* 2017, 8:15741.
51. Garmy-Susini, B, Varner, JA: Roles of integrins in tumor angiogenesis and lymphangiogenesis. *Lymphat Res Biol.* 2008, 6(3-4):155-163.
52. Lugarno,R, Ramachandran, M, Dimberg, A: Tumor angiogenesis, consequences, challenges and opportunities. *Cell Molec Life Sci* 2020, 77(9):1745-1770.
53. Li, T, Yang, J, Zhao, Q, He, Y: Molecular regulation of lymphangiogenesis in development and tumor microenvironment. *Cancer Microenviron* 2012, 5:549-560.
54. Podach, R: The role of lymphngiogenesis and angiogenesis in tumor metastasis. *Cell Oncol* 2016, 39(5):397-410.
55. Saman, H, Raza, SS, Uddin, S, Rasul, K: Inducing angiogenesis, a key step in cancer vascularization, and treatment approaches. *Cancers* 2020, 12(5):1172.

TABLES AND FIGURES WITH LEGENDS

Table 1. Normal Parathyroid, Adenoma, Atypical Tumor, Multiglandular Adenoma and Carcinoma Normal Glands (5)

Case	Age/Sex	Weight (4 glands)	Slide Sizes (cm)
1	51/F	130 mg	0.4 x 0.3 cm
2	53/M	160	0.5 x 0.3
3	56/F	220	0.8 x 0.4
4	66/F	100	0.3 x 0.2
5	71/M	140	0.4 x 0.3
Mean	59.4	150	0.5 x 0.3
SE	4.3	22.3	0.1 x 0.03

Adenomas (12)

1	29/M	1.2 g	1.0 x 0.6 cm
2*	36/M	1.0	1.4 x 0.6
3	43/F	3.0	1.4 x 1.0
4	45/F	1.0	1.5 x 0.6
5*	47/F	0.5	0.8 x 0.5
6	50/F	1.8	1.2 x 0.8
7*	51/F	4.8	2.0 x 1.5
8	53/M	1.5	0.8 x 0.4
9	57/F	1.5	0.8 x 0.6
10	67/F	0.6	0.6 x 0.5
11	69/M	3.6	1.5 x 1.2
12	77/F	1.5	0.8 x 0.6
Mean	52.0	2.1	1.4 x 0.7
SE	4.0	0.4	0.1 x 0.1

*: Normal rim was attached to adenoma.

Multiglandular Adenoma (6)

1	26/F	2.7 g (4 glands)	1.0 x 0.6 cm
2	45/M	4.5	1.2 x 0.7
3	51/F	4.3	1.3 x 0.8
4	56/F	1.5	0.8 x 0.6
5	66/F	7.5	1.5 x 1.0
6	74/F	7.5	1.5 x 1.2
Mean	53	4.7	1.2 x 0.8
SE	7	1.0	0.1 x 0.1

Atypical Tumor (1)

1	81/M	4.5 g	1.5 x 1.2 cm
---	------	-------	--------------

Carcinomas (2)

1	44/M	6.0 g	1.8 x 1.5 cm
2	58/F [#]	2.0	1.3 x 0.6

[#]: Lymph node metastasis

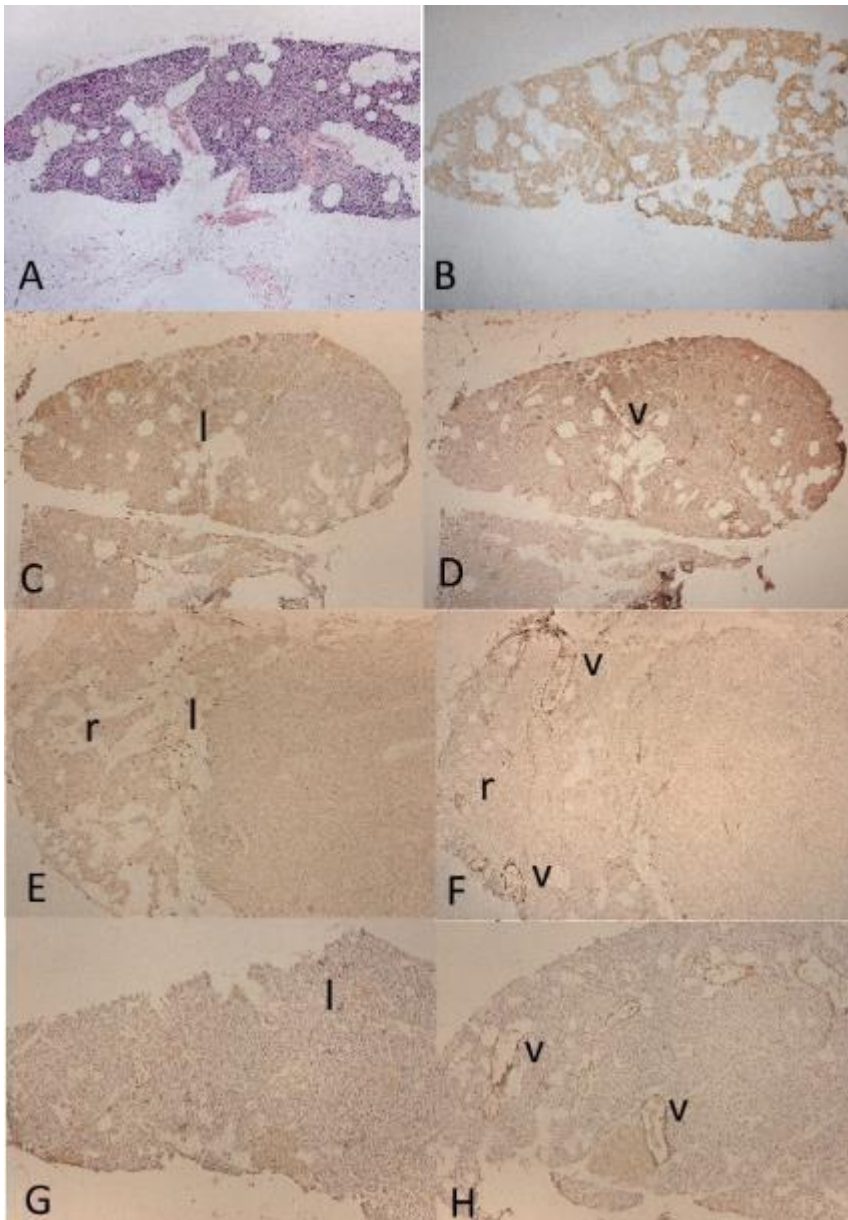


Figure 1. Case 1: Normal gland, Case 4: Adenoma, and Case 3: MMA

The normal parathyroid gland (Case 1) contained about 20% fibroadipose tissue (A) and was strongly positive for PTH (B). It also contained a few smallest linear lymphatic vessels (C) and several round, slightly larger blood vessels, measuring 120 x 15 μm (D). In Case 4, the adenoma was attached to a normal rim, containing about 50% fibroadipose tissue. This area featured a few smallest lymphatic vessels and numerous smallest blood vessels between the rim and the adenoma

(E and F). Case 3 (MMA) revealed several smallest lymphatic vessels (G) and multiple dilated, large blood vessels (120 x 15 μm) that were proportionate to the larger adenoma, with no fibroadipose stroma present (H).

l: lymphatic vessel, r: normal rim, v: vein

A: H&E, B: PTH, C, E, and G: LYVE-1, B, D, F, and G: vWF immunostained

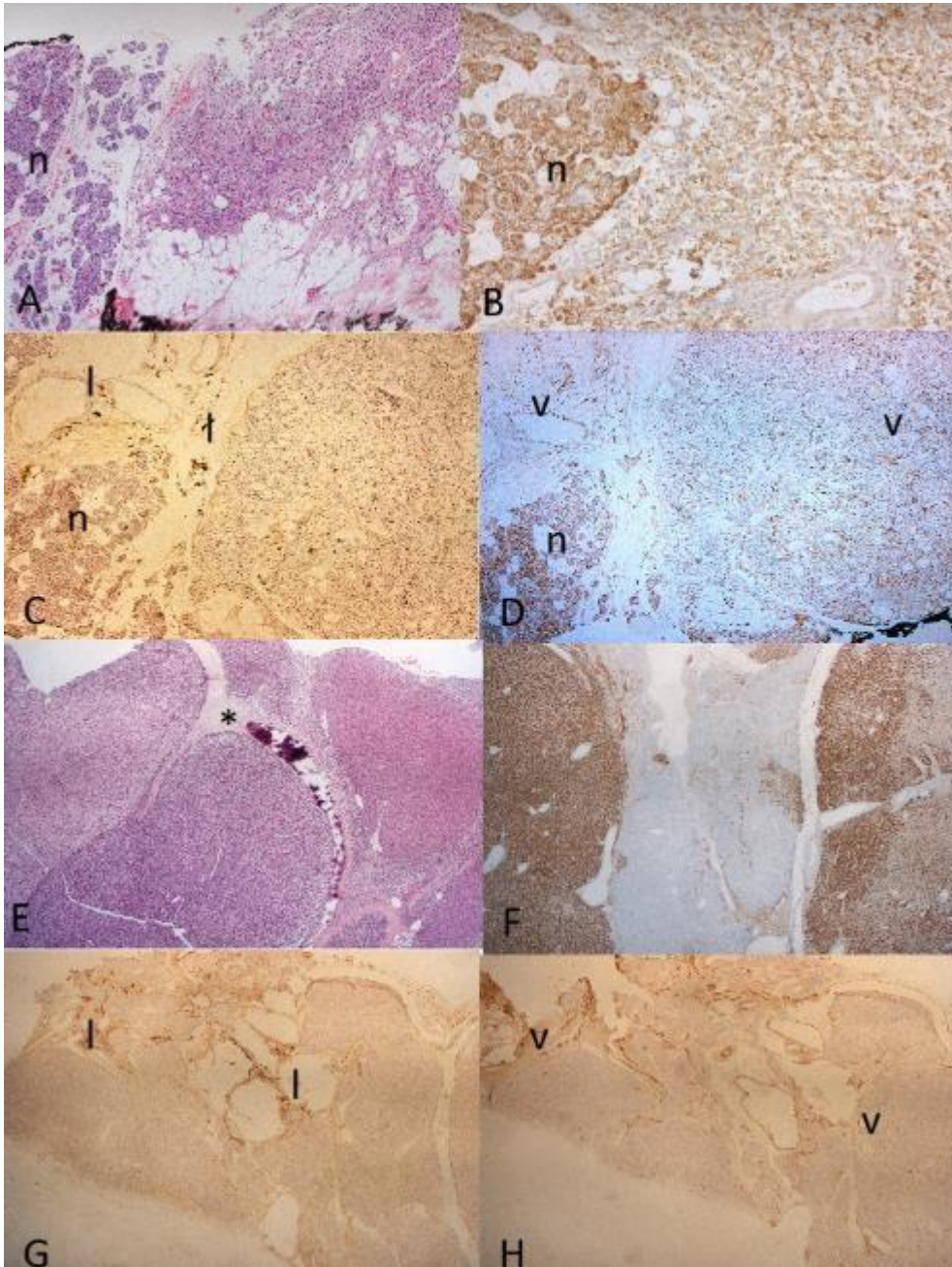


Figure 2. Case 7: Adenoma and Case 5: MMA

In Case 7, the adenoma, which weighed 4.8 g, was composed of cells with amphophilic cytoplasm and prominent nuclei. This adenoma was less immunostained for PTH than the adjacent normal rim (A and B). Several large, dilated blood vessels, measuring 500 μm x 200 μm , were observed, with small linear lymphatic vessels located perivascularly between the adenoma and the normal gland (C and D). In Case 5 (MMA), the adenoma was separated from the surrounding tissue by a thin fibrous band where stromal calcification was present (E). The adenoma consisted of lobules that were alternately strongly positive and negative for PTH immunostaining (E). Additionally, large, dilated blood vessels, measuring 1000 μm x 500 μm , and small perivascular linear lymphatic vessels were observed inside the capsule (G and H).

l: lymphatic vessel, n: normal parathyroid, v: blood vessel

A and E: H&E, B and F: PTH, C and G: LYVE-1, D and H: vWF immunostained

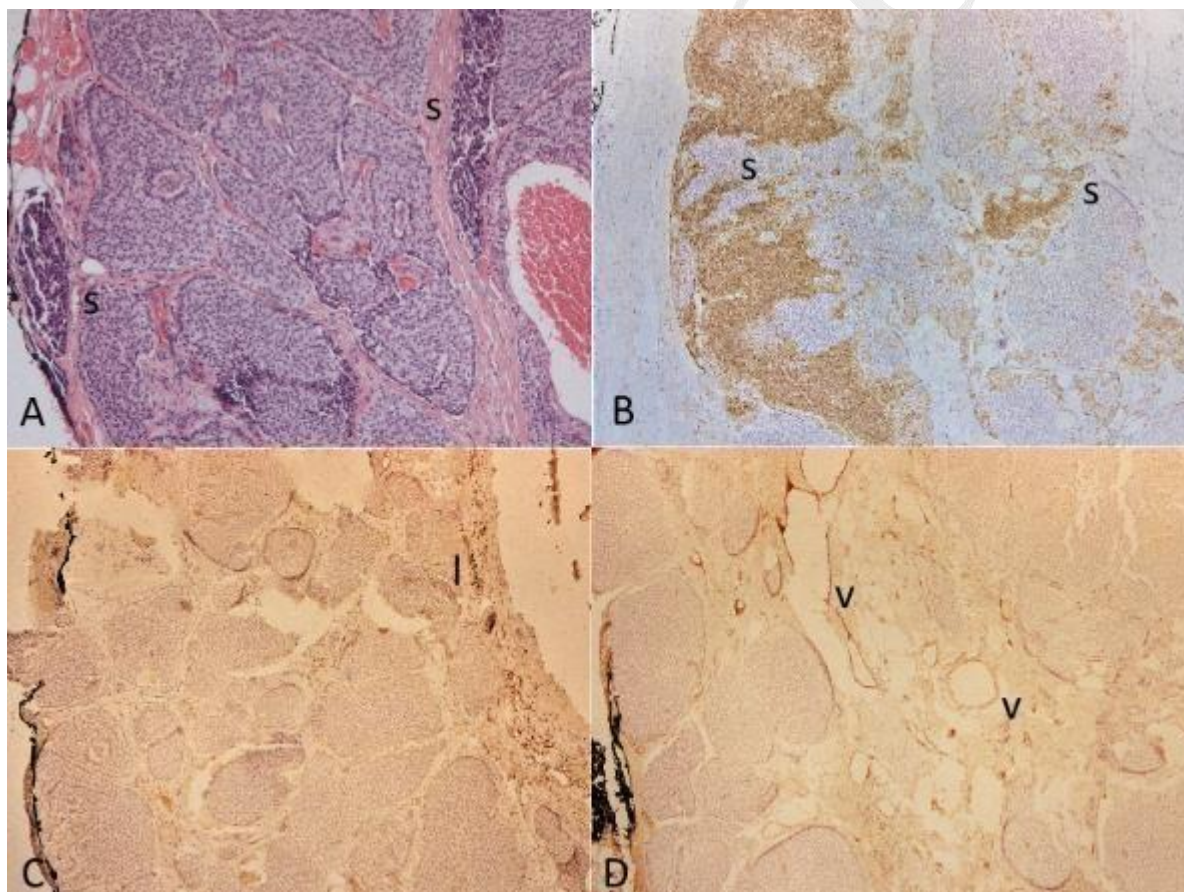


Figure 3. Atypical tumor

The atypical tumor consisted of two distinct lobular patterns: small dense cell lobules with dense

chromatin and small nuclei, and amphophilic cell lobules with larger cytoplasm. These two types of lobules were separated by thick fibrous bands (A). The small dense cell lobules, which were primarily located at the tumor's outer margin, were diffusely and strongly immunostained for PTH. In contrast, the amphophilic cell lobules with larger cytoplasm, nuclei, and nucleoli were PTH-negative (A and B). The tumor also contained numerous large blood vessels, measuring 500 μm x 200 μm , within a thin fibrous stroma, and many small linear lymphatic vessels within the broader fibrous stroma (C and D).

l: lymphatic vessel, s: small cell lobule, v: blood vessel

A: H&E, B: PTH, C: LYVE-1, D: vWF immunostained

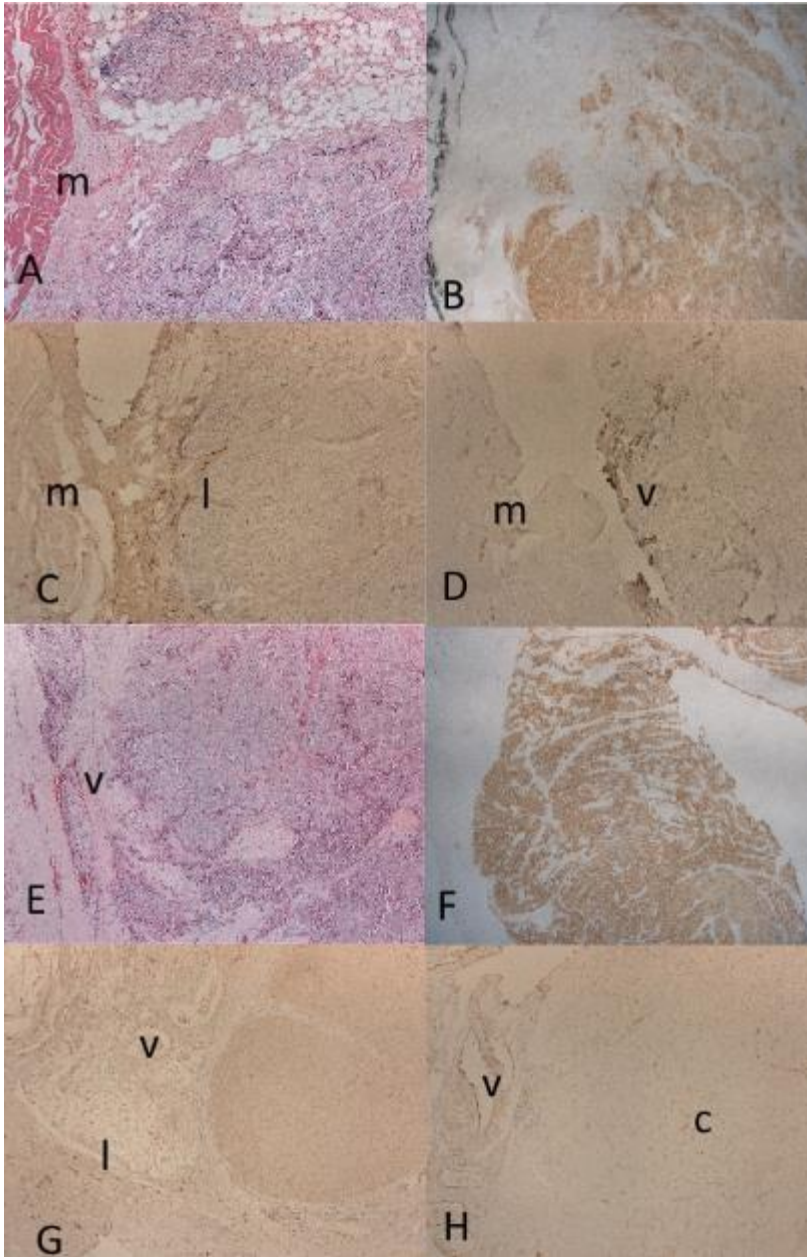


Figure 4. Case 1: Primary carcinoma and Case 2: Metastatic carcinoma in lymph node

In Case 1, the primary carcinoma invaded the neck skeletal muscle (A), which was diffusely and strongly immunostained for PTH (B). Numerous smallest lymphatic vessels (C) and numerous small to smallest blood vessels were observed adjacent to the invading tumor margin (D). In Case 2, the metastatic lymph node revealed tumor emboli at the periphery of the node (E). The cancerous tissues were diffusely and strongly immunopositive for PTH (F). At the peripheral margin of the lymph node, there were dozens of smallest lymphatic vessels and a few large blood vessels,

measuring 500 μm x 200 μm , while the entire lymph node was diffusely infiltrated by small blood vessels (H).

l: lymphatic vessel, m: skeletal muscle, v: vein, c: capillaries

A and E: H&E, B and F: PTH, C and G: LYVE-1, D and H: vWF immunostained

RELATED ARTICLES PUBLISHED IN BJBMS

[Immunohistochemical study of dental pulp cells with 3D collagen type I gel in demineralized dentin tubules in vivo](#)

Sultan Zeb Khan, BJBMS, 2020